ELSEVIER

Contents lists available at ScienceDirect

Fuel Processing Technology

journal homepage: www.elsevier.com/locate/fuproc





Applied smouldering for co-waste management: Benefits and trade-offs

Tarek L. Rashwan ^{a,b,c,*}, Taryn Fournie ^a, Megan Green ^a, Alexandra L. Duchesne ^{a,d}, Joshua K. Brown ^{a,d}, Gavin P. Grant ^d, José L. Torero ^e, Jason I. Gerhard ^a

- ^a Department of Civil and Environmental Engineering, The University of Western Ontario, London, Ontario N6A 5B9, Canada
- b Department of Civil Engineering, Lassonde School of Engineering, York University, Toronto, Ontario M3J 1P3, Canada
- ^c School of Engineering & Innovation, The Open University, Milton Keynes MK7 6AA, UK
- d Savron. Toronto, Ontario M8X 1Y9, Canada
- ^e Department of Civil, Environmental and Geomatic Engineering, University College London, London WC1E 6BT, UK

ARTICLE INFO

Keywords: Smouldering combustion Waste-to-energy Sewage sludge Process scale-up Gasification Biomass

ABSTRACT

Smouldering combustion is emerging as a valuable application for many environmentally beneficial purposes, including waste-to-energy. While many applied smouldering systems rely on small fractions of fuel mixed within inert porous media (IPM) like coarse grain silica sand, there is also an opportunity to pursue co-waste management with much higher fuel loadings. This study explores these co-waste systems by blending non-smoulderable wastes (e.g., sewage sludge) with smoulderable wastes (e.g., construction waste woodchips) to form porous solid fuels (PSFs). Key differences between these IPM and PSF systems were identified by contrasting the temperature profiles in space and time, specific mass loss rates, and emissions profiles across experiments in multiple reactors (with 0.054, 0.080, and 0.300 m radii). For example, the PSF systems exhibited higher throughputs, a more straightforward path towards continuous operation, improved scalability, and higher production of potentially useful by-products (e.g., CH4, H2) than the IPM systems. However, the PSF systems were more sensitive to extinction and exhibited lower fuel moisture content limitations than the IPM systems. Altogether, this study illuminates the benefits and trade-offs of co-waste smouldering.

One file containing supplementary material is available.

1. Introduction

1.1. Applied smouldering combustion

Smouldering combustion is emerging as a valuable application for many environmentally beneficial purposes such as: (*i*) land remediation [1], (*ii*) hazardous liquid management [2,3], (*iii*) decentralized sanitation [4,5], (*iv*) pyrolysis/torrefaction [6–10], (*v*) wastewater sludge treatment [11–13], (*vi*) organic waste treatment [14–16], and (*vii*) resource recovery/generation [17–20]. In all these cases, smouldering can be harnessed to generate energy from traditionally problematic wastes, such as those with high moisture contents (e.g., biomass sludges [15,21,22]) and low volatility (e.g., coal tars and heavy oils [2,3,23–25]).

Smouldering is a flameless form of combustion where oxygen in the

pore space transports and reacts with the surface of the condensed phase fuel [26,27]. Smouldering is commonly seen in a traditional charcoal barbecue. In most contexts, the rate of energy production is hypothesized to be limited by local oxygen transport in the pore space [26–29], though many smouldering models assume the process is limited by chemistry [30,31]. The interplay between chemistry and local mass transport is not yet well-understood in most smouldering systems and warrants more attention [26]. Regardless, if the rate of energy production near the reactions exceeds the rate of energy lost, smouldering will proceed in a "self-sustaining" manner. Within the context of a porous medium, heat and mass transfer can be represented by diffusive approximations and therefore the characteristic time of heat generation and heat losses are equivalent [26]. Combustion chemistry and radiation cannot be approximated in this manner in flaming combustion because they are much faster processes than diffusive heat and mass transfer. This means that smouldering, as opposed to flaming, is considered energy-efficient, as minimal external energy is needed to operate, and ranks highly in sustainability metrics [32]. This is beneficial for wastes

^{*} Corresponding author at: School of Engineering & Innovation, The Open University, Milton Keynes MK7 6AA, UK.

E-mail addresses: tarek.rashwan@open.ac.uk (T.L. Rashwan), tfourni4@uwo.ca (T. Fournie), mgreen87@uwo.ca (M. Green), aduchesne@savronsolutions.com

(A.L. Duchesne), jkbrown@savronsolutions.com (J.K. Brown), ggrant@savronsolutions.com (G.P. Grant), j.torero@ucl.ac.uk (J.L. Torero), jgerhard@uwo.ca

(J.I. Gerhard).

Nomenclature		PSF SH	Porous solid fuel Sunflower husks
AD C CEMS CP DT DRUM GAC IPM LAB LAB2	Anaerobic digestate Centreline Continuous emissions measurement system Coffee pulp Dimensionless time Oil-drum sized reactor (0.300 m radius) Granular activated carbon Inert porous media Large laboratory reactor (0.080 m radius) Small laboratory reactor (0.054 m radius)	SS TC THCs WC Latin let m t v _{cool} v _{oxid}	Municipal sewage sludge Thermocouple Total Hydrocarbons Construction waste woodchips
LTNE MC MS MW OS P	Local thermal non-equilibrium Moisture content (wet mass basis) Macadamia nut shells Mushroom waste Oil sludge Plenum Pulp and paper digestate	Subscrip f i ig off	Final Initial Ignition Heater off

contaminated with recalcitrant compounds with few disposal options, e. g., soil contaminated with *per*- and polyfluoroalkyl substances [33].

In many smouldering applications, the system is comprised of the fuel/waste mixed within an inert porous media (IPM) – such as silica sand. The IPM offers many supports for smouldering, including good air permeability for oxygen delivery, high specific surface area for reaction, and efficient heat transfer within the system [23,26,34]. Furthermore, the addition of IPM can stabilize the reaction front [35] and allow higher moisture content (MC) waste to be managed through recycling the released reaction energy. Indeed, multiple studies have shown that increased IPM fractions can stretch the MC limit to 75–85% for various biomass sludges [21,22,34]. However, there are downsides to mixing wastes with sand prior to treatment, e.g., the sand management before and after treatment and considerable time is required to cool down the system after treatment – both of which add engineering complexity [36,37].

Gasification and pyrolysis systems exhibit numerous technical similarities to applied smouldering systems. In these systems, the use of catalytic and non-catalytic IPM can improve system performance by driving higher gas production (e.g., H_2 and CO) [38,39], lowering tar production [40], and improving heat transfer rates [41]. However, these systems routinely use porous solid fuels (PSFs) alone without IPM, e.g., from agricultural, forestry, and municipal sources [42]. Using PSFs directly increases throughput and simplifies handling; however, these systems exhibit lower MC% limits than IPM smouldering systems. For example, updraft gasifiers using PSFs, which are similar to PSF smouldering systems, typically require fuels with $\lesssim 60\%$ MC [43]. This suggests, while there are benefits in replacing IPM in applied smouldering systems with PSFs, there are also trade-offs.

1.2. Smouldering zones in IPM and PSF systems

Smouldering is characterized by a series of interdependent *zones* that evolve in space and time. These zones foster a dynamic thermal system, where the importance of each zone varies depending on the fuel type, porous media properties, air flux, etc. [26,44]. The key zones common to smouldering systems are the *inert heating*, *reaction*, and *cooling* zones. These zones are similar to those found in gasifiers and pyrolizers [42,43]. While most applied smouldering systems use IPM, many pyrolizers and gasifiers (as well as smouldering fire problems) involve PSF systems, which inform Fig. 1.

The inert heating zone is an endothermic, reaction-free region characterized by phase change processes (e.g., water phase change [45])

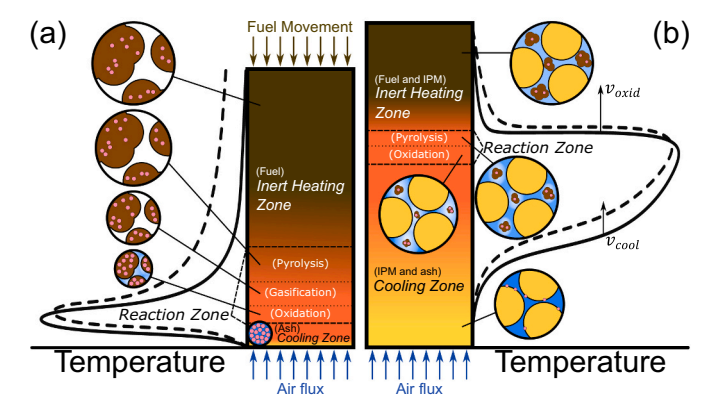


Fig. 1. Key zones in applied smouldering systems using either: (a) porous solid fuel (PSF) or (b) inert porous media (IPM). The *cooling, reaction,* and *inert heating zones* are highlighted for further discussion and the reaction zone is further subdivided into the oxidation, gasification, and pyrolysis regions. The solid and dashed lines indicate the conceptual solid and gas phase temperatures, respectively, due to local thermal non-equilibrium. The callouts depict characteristic representative elementary volumes from each system, where the changing size depicts the shrinkage throughout the system and the colours approximate the oxygen distribution in space, i.e., white indicates oxygen-depleted areas. The smouldering and cooling velocities (ν_{oxid} and ν_{cool} , respectively) are also labelled, where $\nu_{oxid} > \nu_{cool}$.

and fuel preheating, driven by the heat transferred upstream from the reaction zone. Local-thermal non-equilibrium (LTNE) drives heat transfer to unreacted fuel [46]. The cooling zone is also reaction-free and is driven by heat transfer between the hot porous media and cool incoming air [47]. Because large fractions of IPM are often used in common applied smouldering systems that support fuel-limited propagation (often >80% of the mixture mass), the cooling zone is fuel-free and, like the inert heating zone, driven by LTNE heat transfer. Moreover, because the smouldering velocity (v_{oxid}) is often larger than the cooling velocity (v_{cool}) in IPM systems, the cooling zone grows throughout smouldering propagation [47-49]. The cooling zone serves a key function: it provides a buffer against extinction from reaction perturbations (i.e., bolsters resilience against the termination of chemical reactions to local heat losses [44,50]), like porous burners [40,51]. However, long cooling zones are also problematic, as they are responsible for: (i) nearly all perimeter heat losses from the system (i.e., an inefficiency) [46,47,52] and (ii) non-uniform air flux (i.e., a liability)

[48,53]. In contrast, the small fraction of inert material in PSF systems (i.e., only ash) fosters a much thinner cooling zone. While this thinner cooling zone minimizes air flow distortions and heat losses from PSF systems, it also leaves the oxidation reactions exposed and therefore more sensitive to thermal perturbations [50].

The reaction zone in IPM systems is often quite thin [O(0.001-0.01 m)] due to the small fuel concentrations [26]. However, PSF smouldering systems (i.e., with larger fuel fractions) foster thicker reaction zones, e.g., fire safety hazards like polyurethane foam [26] and peat soil [30,54]. These PSF systems often foster oxygen-limited smouldering propagation. In all cases, the chemical activity in the smouldering reaction zone is complicated by competing endothermic and exothermic reactions [30,31,55]. Though, in forward smouldering systems (i.e., air flow and smouldering spread in the same direction), the endothermic reactions (e.g., pyrolysis) generally proceed ahead of the exothermic reactions (e.g., oxidation) [26].

Fig. 1 shows that, while these characteristic zones are common to IPM and PSF smouldering systems, there are important differences in their sizes and intensities - especially in the cooling and reaction zones. In PSF systems, less heat is stored in the cooling zone than in IPM systems, and therefore a greater fraction of the combustion energy is transferred forward to drive downstream endothermic reactions (i.e., pyrolysis and gasification in Fig. 1a). Moreover, the reaction zone in the PSF systems facilitate a wider range of degradation reactions than in IPM systems. Under well-tailored conditions, it can drive more gasification (e.g., char gasification) between the oxidation and pyrolysis reactions; essentially, the key processes in an updraft gasifier [42]. In part, these differences are due to the comparatively large fuel loading in PSF systems, which fosters anoxic conditions at sufficiently high temperatures to favour gasification. Given the lower fuel loadings, these conditions are not attained in most IPM systems. Fig. 1 also overlays the characteristic solid and gas phase temperatures, the expected oxygen distribution in the pore space, and the shrinkage in both systems (which keeps the PSF systems' reaction zone nearly fixed in space in the as fuel moves downward). The characteristic changes in the zones in IPM or PSF smouldering systems are anticipated to govern the benefits and tradeoffs of each approach, but very few applied smouldering studies contrast them.

This study presents a quantitative analysis of 44 experiments across different reactor scales exploring the use of smouldering for co-waste management. The focus is primarily on sewage sludge mixed with waste construction woodchips, emphasizing a porous solid fuel (PSF). By contrasting these results with treatment of sewage sludge mixed with sand (i.e., an inert porous media, IPM), valuable insight is drawn between these systems that govern their benefits and trade-offs. The conclusions support designing improved applied smouldering and related thermal conversion systems including gasifiers and pyrolizers.

2. Methodology

Table 1 details the experimental conditions from 44 smouldering experiments performed with a range of wastes: municipal sewage sludge (SS), agricultural waste [macadamia nut shells (MS), mushroom waste (MW), coffee pulp (CP), and sunflower husks (SH)], construction waste woodchips (WC), pulp and paper digestate (PP), anaerobic digestate (AD), and oil sludge (OS). These wastes were smouldered alone (Single Wastes, Table 1), mixed with sand in IPM systems, or combined in PSF co-waste experiments (Co-Wastes, Table 1). The PSF co-waste systems aimed to combine wastes that could not smoulder alone (i.e., oil and sewage sludges) with smoulderable wastes (i.e., construction waste woodchips, agricultural waste, and pulp and paper digestate) to form smoulderable mixtures. Most of the discussion below is focused on the sewage sludge PSF and IPM experiments with woodchips and sand, respectively, performed in the laboratory reactor (LAB: 0.08 m radius) and oil-drum sized reactor (DRUM: 0.3 m radius). Experimental measurements included: temperature histories with thermocouples (TCs),

emissions (CO, CO₂, total hydrocarbons, CH₄, H₂, and O₂), and continuous mass loss. All experiments followed established applied smouldering experimental methods [23,24,34,49,53,56]. Though these experiments used varying setups and ignition procedures, the smouldering behaviour examined in this study was unaffected by these differences [53]. See additional experimental information, characterization, and methodology details in the Supplementary Materials, Section S.1.

3. Results and discussion

3.1. Temperature profiles in IPM and PSF systems

Table 1 presents key smouldering results that demonstrate many cowaste mixtures supported self-sustaining smouldering (i.e., sewage sludge mixed with woodchips and agricultural wastes) and many waste streams supported smouldering alone (i.e., agricultural wastes, pulp and paper digestate, and anaerobic digestate). Note that, the wet fuel mass fractions are presented in the Experimental Conditions and the fuel MC% and ash% were evaluated on wet mass bases (i.e., only the wet fuel fraction for the IPM experiments and the entire mixtures for the PSF experiments). These experiments highlight a wide range of conditions with different wastes and mixtures that support self-sustaining smouldering. Moreover, they reveal key differences between IPM and PSF systems. For example, the MC limit observed in the PSF experiments using woodchips and sewage sludge (i.e., between 64% and 71% from LAB PSF1 and PSF5, respectively) align with the updraft gasifier literature, \$\leq\$ 60-65\% [43]. The IPM experiments also demonstrate selfsustaining smouldering was achievable with mixtures using >74% MC, which also agrees with the applied smouldering literature [19]. However, a few PSF experiments (i.e., LAB PSF12-14) achieved selfsustaining smoulder with a higher MC (75%) using anaerobic digestate. In part, this result is due to the higher ash content in anaerobic digestate (15%) than the woodchips/sewage sludge mixtures (6.3-8.0%), which fostered improved energy recycling between the cooling and reaction zones - common in IPM systems. However, many other variables also affect this limit (e.g., fraction of bound water, surface area for reaction, calorific content, fixed/volatile carbon fractions).

Fig. 2 illustrates the temperatures measured along the centreline at three snapshots in time in three repeat IPM experiments (DRUM IPM1, IPM2, and IPM3) and two different PSF experiments (DRUM PSF1 and PSF2; see Table 1 for extra details). The dimensionless time (DT) was defined by the ignition and end of smouldering times to compare experiments with varying bed lengths and processing rates [57] (see details on evaluating these times in the Supplementary Materials, Section S.4). Note that dimensionless analyses can help elucidate many complicated phenomena in smouldering systems, such as the effect of heat losses with scale and the transition from robust to weak smouldering [47,49]. These experiments facilitated self-sustaining smouldering but characteristically different temperature profiles, which corroborate Fig. 1. As shown in Fig. 1a, the peak temperatures in the PSF systems in Fig. 2a-c (corresponding approximately to the beginning of the reaction zone locations) were nearly fixed around 0.1-0.2 m up the column. This is because the resulting ash consolidated in the cooling zone below the peak temperatures and fuel from above tumbled into the reaction zone. On the other hand, Fig. 2d and e shows that that smouldering reaction zone travelled up the system as the IPM formed a fixed matrix that fostered smouldering propagation. These differences highlight one practical distinction of PSF systems: they offer a straightforward path towards continuous operation as only small fractions of ash need to be removed from the system over time, as opposed to larger fractions of sand or other inert material in IPM systems (this point is further discussed below in Section 3.2).

Fig. 2 also shows that, in the context of the TC resolution, the cooling zones in the PSF experiments (< 0.1 m in Fig. 2a-c) were much thinner in than in the IPM experiments ($\sim 0.1 \text{ to } 0.3\text{--}0.4 \text{ m in Fig. 2d}$ and f,

Table 1 Experimental conditions and key smouldering front results.

Experimental conditions				Smouldering front results				
Experiment ¹	Porous solid fuel or sand: non-smoulderable fuel [g:g] LAB $\pm 0.3\%$ DRUM $\pm 2\%$ $MC \pm 0.1\%$, $Ash \pm 0.1\%$	Darcy air flux (21.1°C, 1 atm) [cm s $^{-1}$] LAB $\pm 3\%$ DRUM	Initial fuel bed height [m] ± 0.003 m	Self- sustaining? [Yes/No/ Borderline]	Mean centreline propagation velocity [cm min $^{-1}$] LAB $\pm 4\%$ DRUM $\pm 10\%$	Mean centreline peak temperature [°C] LAB ±1% DRUM ±4%	Mean $CO(\text{vol.}\%)$ $CO_2(\text{vol.}\%)$ LAB $\pm 10\%$ DRUM $\pm 2\%$	
		$\pm 2\%$						
Porous solid	uel experiments (co-wastes)							
DRUM PSF1	0.4 (WC): 1 (SS) 64, 8.0	2.5-5.0	0.434	Y	_	796	0.16 ^a	
DRUM PSF2	0.7 (WC): 1 (SS) 48, 12	0.8-5.0	0.537	Y	_	978	0.24^{a}	
LAB PSF1	0.4 (WC): 1 (SS) 64, 7.9	5.0–6.0 ^b	0.245	Y	_	799	_a	
LAB PSF2	0.7 (WC): 1 (SS) 49, 11	5.0–6.0 ^b	0.170	Y	_	655	_a	
LAB PSF3	0.4 (WC): 1 (SS) 56, 9.6	5.0–6.0 ^b	0.500	Y	_	896	_a	
LAB PSF4	0.4 (WC): 1 (SS) 56, 9.6	5.0-6.0 ^b	0.265	Y	_	898	_a	
LAB PSF5	0.4 (WC): 1 (SS) 71, 6.3	5.0-6.0 ^b	0.185	N	_	_	_a	
LAB PSF6	1.3 (WC): 1 (SS) 38, 12	5.0-6.0 ^b	0.135	Y	_	1022	_a	
LAB PSF7	5.0 (MW): 1 (SS) 22, 21	5.0-6.0 ^b	0.140	Y	_	1061	_a	
LAB PSF8	2.0 (MS): 1 (SS) 34, 4.9	5.0–6.0 ^b	0.115	Y	_	1164	_a	
LAB PSF9	9.0 (PP): 1 (OS) 59, 23	5.0	0.400	В	_	923	_a	
LAB PSF10	2.5 (PP): 1 (OS) 47, 18	5.0	0.400	N	_	_	_a	
LAB PSF11	7.0 (PP): 1 (SS) 66, 23	5.0	0.400	N	-	-	_a	
	uel experiments (single wastes)							
LAB PSF12	AD-only 75, 15	2.5	0.350	Y	_	752	0.24	
LAB PSF13	AD-only 75, 15	5.8	0.324	Y	_	765	_a	
LAB PSF14	AD-only 75, 15	1.7-12.5	0.288	Y	_	872	_a	
LAB PSF15	PP-only 65, 25	5.8	0.290	Y	_	882	0.20	
LAB PSF16	SS-only 75, 7.2	5.0–6.0 ^b	0.203	N	_	_	_a	
LAB PSF17	CP-only 1.0, 9.2	5.0–6.0 ^b	0.105	Y	_	1240	_a	
LAB PSF18	MS-only 10, 3.9	5.0–6.0 ^b	0.100	Y	_	1161	_a	
LAB PSF19	MW-only 7.5, 23	5.0–6.0 ^b	0.100	Y	_	1247	_a	
LAB PSF20	SH-only 5.9, 4.3	5.0–6.0 ^b	0.173	Y	_	1160	_a	
LAB PSF21	WC-only 1.0, 6.4	5.0–6.0 ^b	0.080	Y	-	1269	_a	
C LAB2 PSF22	WC-only 11, 16	2.5	0.395	Y	1.2	1228	_a	
-	nedia experiments (sewage sludge							
DRUM IPM1	6.5:1 72, 6.4	5.0	0.621	Y	0.27	500	0.22	
DRUM IPM2	6.5:1 72, 7.6	5.0	0.610	Y	0.23	475	0.21	
DRUM IPM3	6.5:1 74, 5.7	5.0	0.592	Y	0.24	481	0.22	
DRUM IPM4	4.5:1 73, 5.9	3.0	0.542	Y	0.14	482	0.16	
DRUM IPM5	4.5:1 <i>75</i> , – ^d	1.0	0.522	Y	0.09	436	0.16	
DRUM IPM6	16:1 40, 14.4	5.0	0.382	Y	0.40	512	0.14	
DRUM IPM7	4.5:1 73, 6.5	5.0	0.641	Y	0.20	528	0.18	
DRUM IPM8	4.5:1 74, 6.5	15	0.612	Y	0.25	459	0.18	
LAB IPM1	6.5:1 72, 7.6	5.0	0.410	Y	0.46	519	0.25	
LAB IPM2	6.5:1 72, 7.6	5.0	0.448	Y	0.48	525	0.25	
LAB IPM3	6.5:1 74, 5.7	5.0	0.440	Y	0.49	524	_a	
LAB IPM4	23:1 3.2, 28	5.0	0.340	Y	0.53	516	0.27	
LAB IPM5	23:1 3.2, 28	4.6	0.283	Y	0.46	569	0.22	
LAB IPM6	4.5:1 <i>75</i> , – ^d	5.0	0.438	Y	0.43	541	0.20	
LAB IPM7	4.5:1 73, 5.4	3.3	0.400	Y	0.33	547	_a	
LAB IPM8 LAB IPM9	4.5:1 <i>7</i> 2, <i>7.4</i> 4.5:1 <i>7</i> 2, <i>8.3</i>	3.3 3.3	0.550 0.428	Y Y	0.32 0.33	564 566	_a _a	
מיח וניוון	7.5.1 /2, 0.5	3.3	0.420	1	0.00	300	_	
Inert porous	nedia experiments (pulp and pape	er or digestate v	vith sand)					
LAB IPM10	(P&P) 3.5:1 34, 16	5.0	0.169	Y	0.73	766	0.26	
LAB IPM11	(AD) 3.3:1 74, 2.5	5.8	0.321	Y	0.62	587	0.29	
LI ID II WITT							_a	

¹ DRUM, LAB, and LAB2 experiments were performed 0.300, 0.080, and 0.054 m radii reactors, respectively.

^a Emissions analyzer was not operational or exceeded the calibration range for a portion of the experiment.

 $^{^{\}rm b}$ The air mass flux was fixed at $5.0~{\rm cm~s^{-1}}$, but the controller exhibited an unusually large error and the actual flow could have been 15-20% higher than anticipated. Therefore, $5.0-6.0 \text{ cm s}^{-1}$ is reported, though the air flux was not changed throughout each experiment.

^c Used a thin laboratory reactor (radius = 0.054 m) and smouldered in a downward orientation (see Supplementary Materials, Fig. S.4).

^d The ash content was not measured.

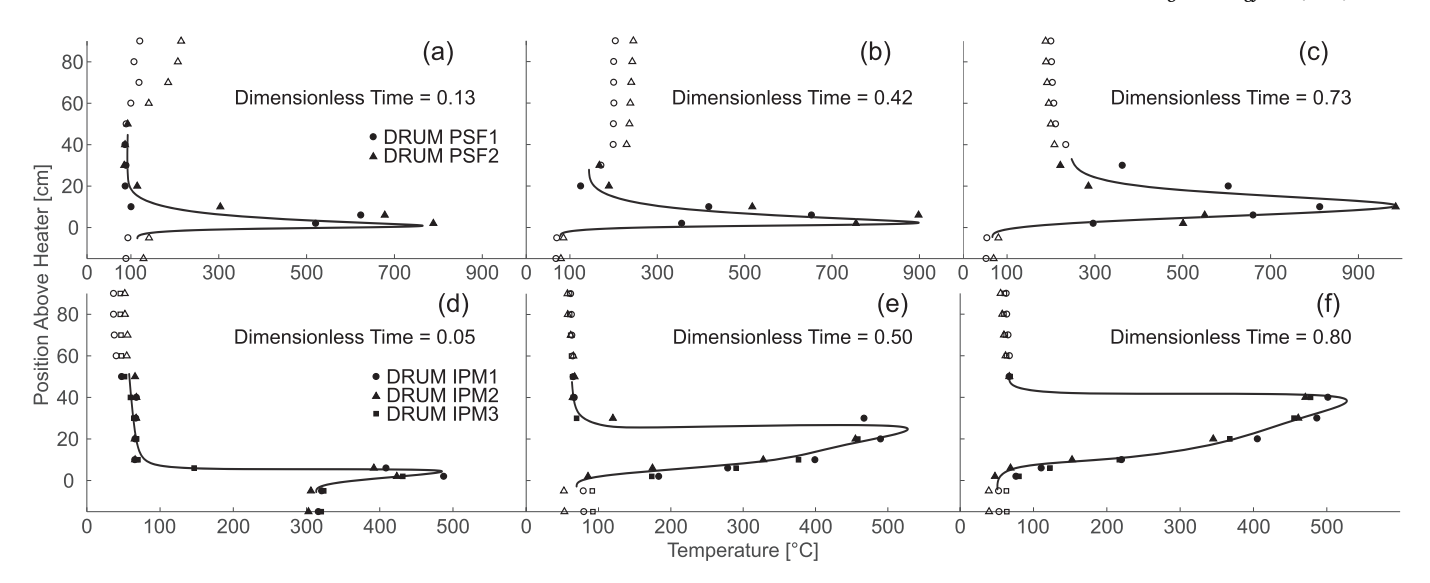


Fig. 2. Centreline temperatures in: (a–c) DRUM PSF1 and PSF2 and (d–f) DRUM IPM1, IPM2, and IPM 3. The legends in (a) and (d) are common to (a–c) and (d–f), respectively. The solid markers indicate the temperatures in the fuel beds, which collapsed over time in DRUM PSF1 and PSF2, and the open markers indicate the emissions temperatures in the air space above the fuel beds. The solid lines illustrate the approximate temperature profiles in the fuel beds.

respectively). These thin cooling zones in the PSF experiments were due to the rapid energy dissipation from the small fractions of ash trailing smouldering. This is a strong contrast to the IPM profiles which developed long cooling zones that grew throughout time based on the system properties – see additional details in the Supplementary Materials, Section S.7. These growing cooling zones are characteristic of IPM smouldering systems, which provide a buffer against reaction perturbations (i.e., a benefit) but can also lead to non-uniform air flux (i.e., a trade-off). Therefore, by reducing the length of the cooling zone in PSF systems, the heat losses behind the front were reduced and the airflow feeding the reactions was more uniform (this benefit is further examined in Section 3.2). However, a trade-off in PSF systems, as mentioned above, is that the reaction zone does not have the stability like in IPM systems due to its thinner cooling zone and it is therefore more sensitive to perturbations that can lead to extinction and process failure.

The reaction zone does not appreciably grow in IPM systems because of the fuel-limited nature of propagation (see extra discussion and data in the Supplementary Materials, Section S.6). In contrast, the reaction zone may grow in PSF systems because propagation is oxygen-limited. Therefore, oxygen-starved reactions (e.g., gasification, pyrolysis) can progress faster than oxidation and stretch the reaction zone. This stretching is common to PSF smouldering systems in the fire safety literature [26], and further discussed below in Section 3.2. Altogether, this reaction zone growth, with increasing fraction of endothermic reactions, can limit peak temperatures and increase the propensity to extinction in PSF systems.

Fig. 2 also shows the peak temperatures in the PSF experiments (700–1000°C throughout DRUM PSF1-2) were higher than the IPM experiments (440–540°C throughout DRUM IPM1-3) due primarily to increased fuel loading. The peak temperatures throughout each experiment were also more variable in the PSF experiments due to the collapsing fuel beds, which caused more chaotic smouldering than in the IPM experiments (see temperature histories in the Supplementary Materials, Section S.5). In addition, the emissions leaving the DRUM reactor were much hotter in the PSF experiments (> 200°C) than the IPM experiments (< 80°C) while the reaction front was appreciably far from the end of the fuel bed (> 0.1 m). These hot emissions in the PSF experiments are uncommon in IPM experiments, the energy released from the reaction zone is quickly transferred to the nearby IPM, even in systems with similarly high peak temperatures (700–1000°C), e.g., using granular activated carbon [33,49,58].

The hot emissions in the PSF experiments are suspected to be due to a

combination of LTNE, permeability heterogeneity, and non-uniform drying in the PSF systems. Locally, a fraction of the energy released by smouldering is transferred to the gas phase in both systems, which then drives preheating ahead of the reactions due to LTNE heat transfer [46,59]. IPM systems typically have a sufficient specific surface area to drive good LTNE heat transfer, but the PSF experiments used larger, clumped fuel particles with a lower specific surface area (see comparison photos in the Supplementary Materials, Section S.1). This distinction is specific to these PSF experiments, as other PSF systems (e.g., polyurethane foam) do have sufficiently high specific surface area [26]. Globally, there is evidence that: (i) mixture heterogeneity and (ii) nonuniform drying also contributed to hot emissions (see additional commentary in the Supplementary Materials, Section S.5). These issues were most pronounced in the DRUM experiments. While care was taken in preparing all mixtures in this study, heterogeneities (e.g., in permeabilities) were inevitable due to the nature of the wastes. These heterogeneities were responsible for some air channelling around smouldering reactions, e.g., as shown by [36,58]. In addition, temperature profiles show that fuel near the reactor walls dried faster than the fuel near the centre (i.e., non-uniform drying), which also contributed to hot air channelling away from the reactor centreline (see Supplementary Materials, Section S.5). Non-uniform drying is hypothesized here to have mainly resulted from non-uniform air flux, i.e., higher air fluxes near the reactor wall due to heat losses. Altogether, these local and global differences led to less efficient heat transfer ahead of the PSF experiments, particularly in DRUM PSF1 and PSF2, with higher smouldering emissions temperatures than all IPM experiments.

Altogether, while the reasons governing the hot emissions in the PSF cannot be fully resolved in these experiments, they are highlighted as an inefficiency, as that lost energy could be used to drive productive activities, e.g., more gasification, higher fuel processing rates, or improve reaction stability. This result also highlights an important benefit in IPM systems, which is that the released reaction energy is more easily recycled when using large fractions of IPM.

3.2. Scalability and semi-continuous operation in PSF systems

Fig. 3a and b show the temperature, mass loss, and specific mass loss rate histories from sewage sludge experiments with woodchips (LAB PSF3) and sand (LAB IPM2). Fig. 3c and d show the temperatures and approximate reaction (i.e., pyrolysis and oxidation) velocities, respectively, from an experiment with only woodchips (LAB2 PSF22). The

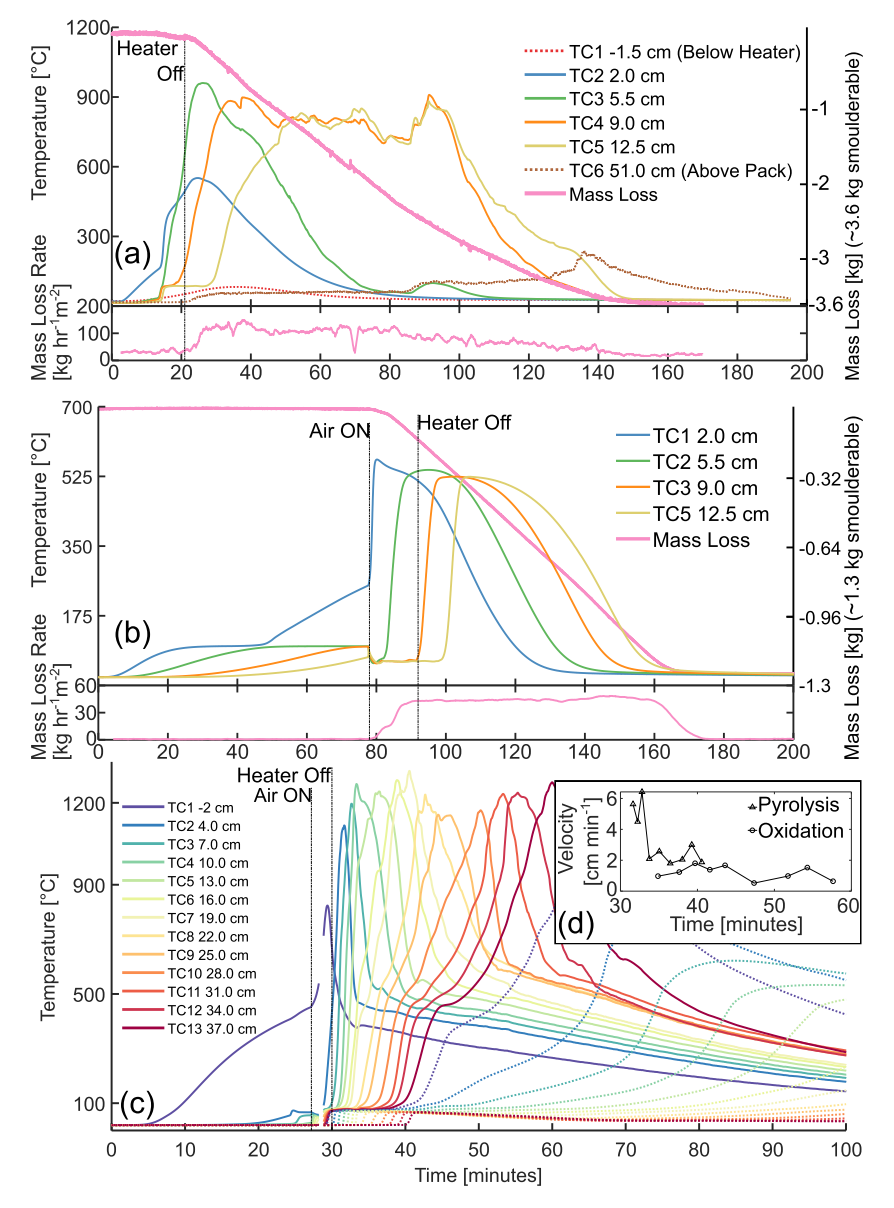


Fig. 3. Temperature, mass loss, and mass loss rate histories from (a) LAB PSF3 and (b) LAB IPM2; and (c) temperature and (d) reaction velocity histories from LAB2 PSF22. The heater-off and air-on times are noted with vertical dashed lines. The dotted lines in (c) note the temperatures in the unreactive clean sand layer from 0.40 to 0.76 m.

pyrolysis and oxidation velocities were estimated from the times when each TC heated above 200°C and reached its peak temperature, respectively. Note that the smouldering and pyrolysis velocities are often very similar in IPM systems, as these reactions typically travel close together (e.g., as seen in the consistent sharp heating rates observed in Fig. 3b) [60]. Self-sustaining smouldering established shortly after the heater was turned off (~ 20, 90, and 27 min in Fig. 3a-c, respectively). Furthermore, practically all fuel was consumed, i.e., > 99% of the smoulderable mass was removed in LAB PSF3 and LAB IPM2, as some mass often remains in the crust around the perimeter [11,53]. However, the median specific mass loss rates were roughly two-fold higher in LAB PSF3 (95 kg hr⁻¹ m⁻², Fig. 3a) than LAB IPM2 (44 kg hr⁻¹ m⁻², Fig. 3b), even though the smoulderable mass loading was seven-fold higher in LAB PSF3 than LAB IPM2. This indicates that, while the mass loss rate increased with fuel-loading, it did not increase proportionally. This result may be due to shifting smouldering propagation control (i.e., from being fuel- to oxygen-limited in IPM to PSF systems, respectively). Like shown in Fig. 2, the higher fuel loading also led to hotter peak temperatures in LAB PSF3 (880-960°C, Fig. 3a) than LAB

IPM2 (520-570°C, Fig. 3b).

Because the reaction zone was nearly stationary in LAB PSF3, the smouldering reactions occurred in single locations for much longer than in LAB IPM2. That is, LAB PSF3's TCs 4 and 5 oscillated near the peak temperatures for approximately 70 and 50 min, respectively, whereas all peak temperatures immediately dissipated in LAB IPM2. In addition, Fig. 3 shows that LAB PSF3 exhibited slower heating rates than LAB IPM2 at the same applied air flux. This is likely due to the wider range of reactions in LAB PSF3, particularly the inclusion of gasification reactions (see Fig. 1). However, unlike the comparisons between DRUM PSF1-2 and DRUM IPM1-3 (Fig. 2), the LAB PSF3 emissions temperatures were cool throughout most of smouldering (< 70°C until 86 min). These cool emissions were common among many LAB PSF experiments, which suggests that the global heat transfer effects (i.e., from mixture heterogeneity and non-uniform air flux) likely governed the hot emissions seen in DRUM PSF1-2. Mixture heterogeneities and non-uniform air flux both worsen in larger reactors [53].

Fig. 3c shows a unique PSF experiment that supported downward forward smouldering; therefore, the fuel did not tumble into the reaction

zone like in all other PSF experiments (as shown in Fig. 1a), but instead the smouldering zones travelled downward. As discussed earlier, this experiment shows two different velocities observed for oxidation and pyrolysis, where the medians from Fig. 4d are 1.2 and 2.6 cm min⁻¹, respectively. Therefore, the reaction zone in this experiment grew over time and became increasingly sensitive to perturbations. This experiment demonstrates some unsteady processes that can lead to problems in PSF systems.

As introduced earlier, a key benefit of PSF systems is their suitability for simple continuous (or semi-continuous) operation. Fig. 4 shows two proof-of-concept, semi-continuous experiments using: (i) sewage sludge mixed with woodchips (LAB PSF4, Fig. 4a) and (ii) anaerobic digestate alone (LAB PSF12, Fig. 4b). These experiments added \sim 1.0 and \sim 0.2 kg batches in Fig. 4a and b, respectively. The last addition of 2.5 kg in Fig. 4b was from adding a clean sand cap (for safety purposes). This allowed \sim 7 kg of fuel to be treated semi-continuously in both LAB PSF4 and PSF12 (approximately two full LAB reactors). The peak temperatures are comparable to other PSF experiments (900 and 750–860°C in LAB PSF4 and PSF12, respectively) and their nearly steady specific mass loss rates (medians 162 and 98 kg hr $^{-1}$ m $^{-2}$ in LAB PSF4 and PSF12, respectively) indicate that the experiments' self-sustaining smouldering did not deteriorate over time.

As these experiments were conducted over short durations for proof-of-concept purposes, the ash accumulation was not a concern. In application, these systems will need to remove the accumulated low permeability ash so that it does not cause a pressure buildup or lead to air channelling. For example, the ash permeability measured in LAB PSF12 (following ASTM D6539-13) was very low (5 \pm 1E-13 m^2) compared to that of the coarse grain sand and sewage sludge ash (e.g., measured from DRUM IPM8 as 3 \pm 1E-10 m^2). A semi-continuous system can also be implemented in IPM systems but requires removing

large fractions of IPM, e.g., [39,61,62]. By contrast, much less inert material needs to be removed from PSF systems (i.e., only fuel ash). Therefore, simpler ash management systems can be integrated into PSF systems than IPM systems.

Another key benefit associated with PSF systems is their scalability. Fig. 5 compares the specific mass loss rates from IPM and PSF experiments in the DRUM reactor against the same experimental conditions in the LAB reactor. The mass loss rates in the PSF and IPM experiments are visualized after ignition and over dimensionless time (DT), respectively (see details in the Supplementary Materials, Section S.4). All experiments were supplied with a Darcy air flux of 5–6 cm s $^{-1}$, where the mass loss rates in DRUM PSF1 and PSF2 are plotted until the air flux was lowered below 5 cm s $^{-1}$ (which was done for safety purposes to control the emissions temperatures).

Fig. 5a underscores the higher processing rates ($> 100 \text{ kg hr}^{-1} \text{ m}^{-2}$) in PSF systems compared to IPM systems (< 50 kg hr⁻¹ m⁻²) due to their higher fuel loading. In addition, the maximum specific mass loss rates from the DRUM PSF experiments (160–210 kg hr⁻¹ m⁻², Fig. 5a) were similar or higher than their LAB counterparts (100–211 kg hr⁻¹ m⁻², Fig. 5a). Conversely, Fig. 5b shows that the DRUM IPM experiments exhibited nearly half the average specific mass loss rates of their LAB counterparts, i.e., 30 and 26 kg hr⁻¹ m⁻² in DRUM IPM1 and IPM3, respectively, versus 46 and 53 kg hr⁻¹ m⁻² in LAB IPM2 and IPM3, respectively. The decrease in processing rates from the LAB to DRUM IPM experiments was due to non-uniform air flux, which caused air channelling along the unreactive crust near the DRUM walls in the long cooling zones [53]. Because the PSF systems did not facilitate long cooling zones, the DRUM PSF experiments processing rates were minimally impacted by non-uniform air flux. This capacity to foster high processing rates is a key advantage of PSF systems.

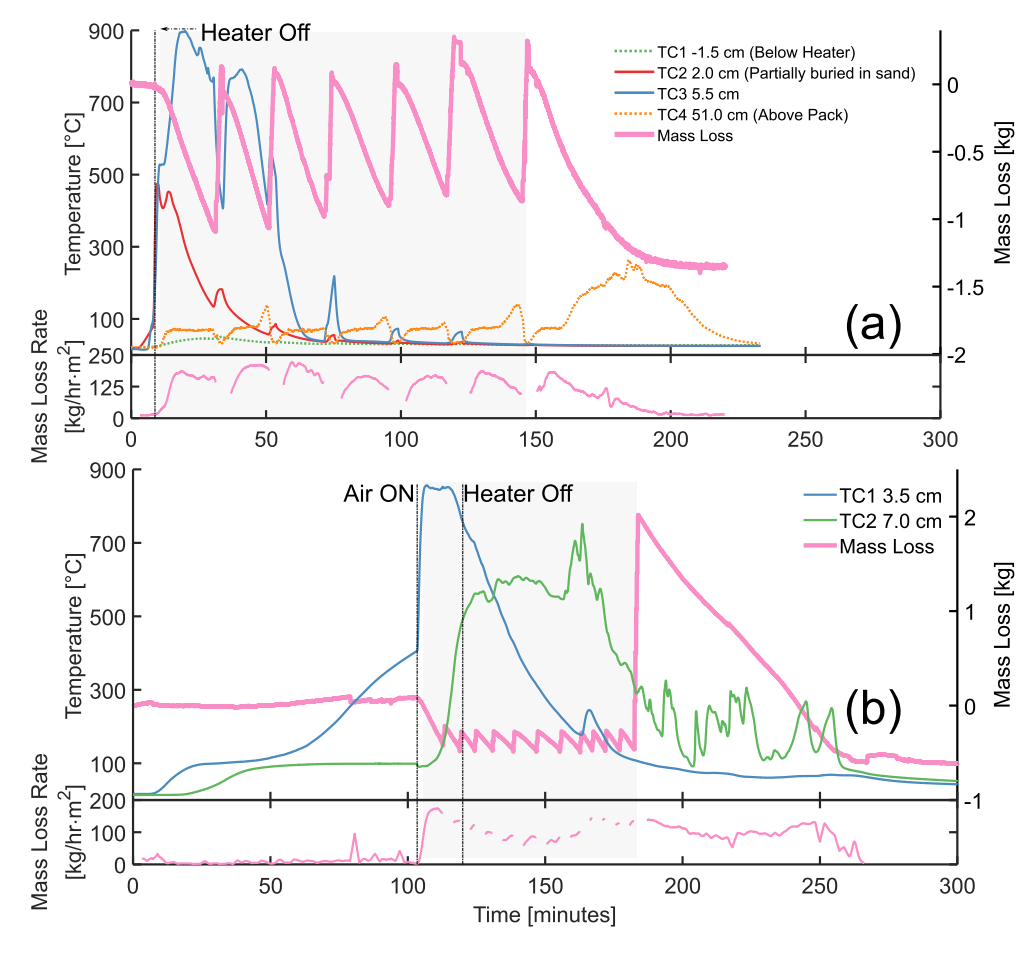


Fig. 4. Temperature, mass loss, and mass loss rate histories from (a) LAB PSF4 and (b) LAB PSF12 showing two proof-of-concept, semi-continuous smouldering experiments. The heater-off times and the air-on time in (b) are noted (as LAB PSF4 and LAB PSF12 used convective and conductive ignition, respectively). Only the bottom 0.055 m and 0.070 m were instrumented with thermocouples (TCs) in (a) and (b), respectively, to minimize the bridging as the fuel bed collapsed downward. The time ranges when new fuel was added semi-continuously are shaded in grey.

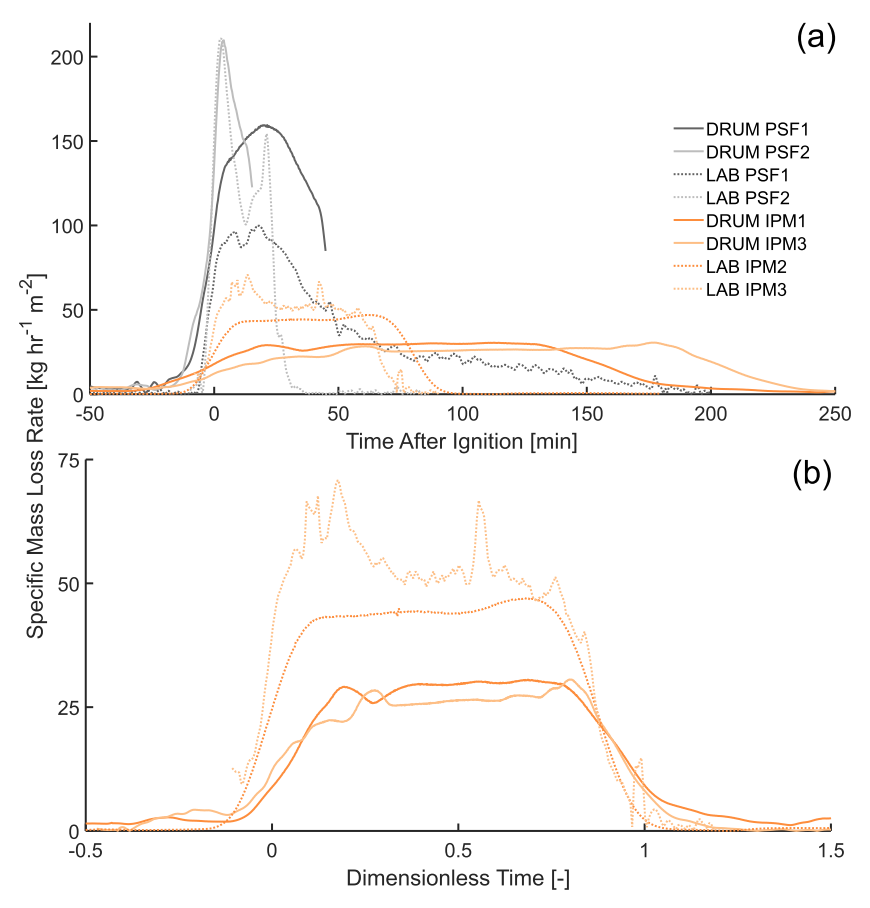


Fig. 5. Specific mass loss rate profiles from (a) LAB PSF1, LAB PSF2, DRUM PSF1, LAB IPM2, LAB IPM3, DRUM IPM1, and DRUM IPM3 plotted after ignition and (b) LAB IPM2, LAB IPM3, DRUM IPM1, and DRUM IPM3 plotted over dimensionless time. Note the LAB and DRUM comparisons used the same experimental conditions, see Table 1.

3.3. The differences in emissions between IPM and PSF systems

Fig. 6a–d show the evolution CO, CH_4 , and total hydrocarbons (THCs), respectively, from select IPM and PSF experiments. These emissions are normalized to the corresponding dynamic CO_2 fractions to account for differences in air flow dilution due to emissions sampling

differences (see the Supplementary Materials, Section S.1). In addition, Fig. 6e shows O_2 measured at the outlet throughout select LAB IPM and PSF experiments, and Fig. 6f shows the H_2 fractions measured from discreet grab samples in DRUM PSF2 at different times in the experiment with different air fluxes. The major data gaps from DRUM PSF1 and PSF2 in Fig. 6a were because the CO measurements initially in these

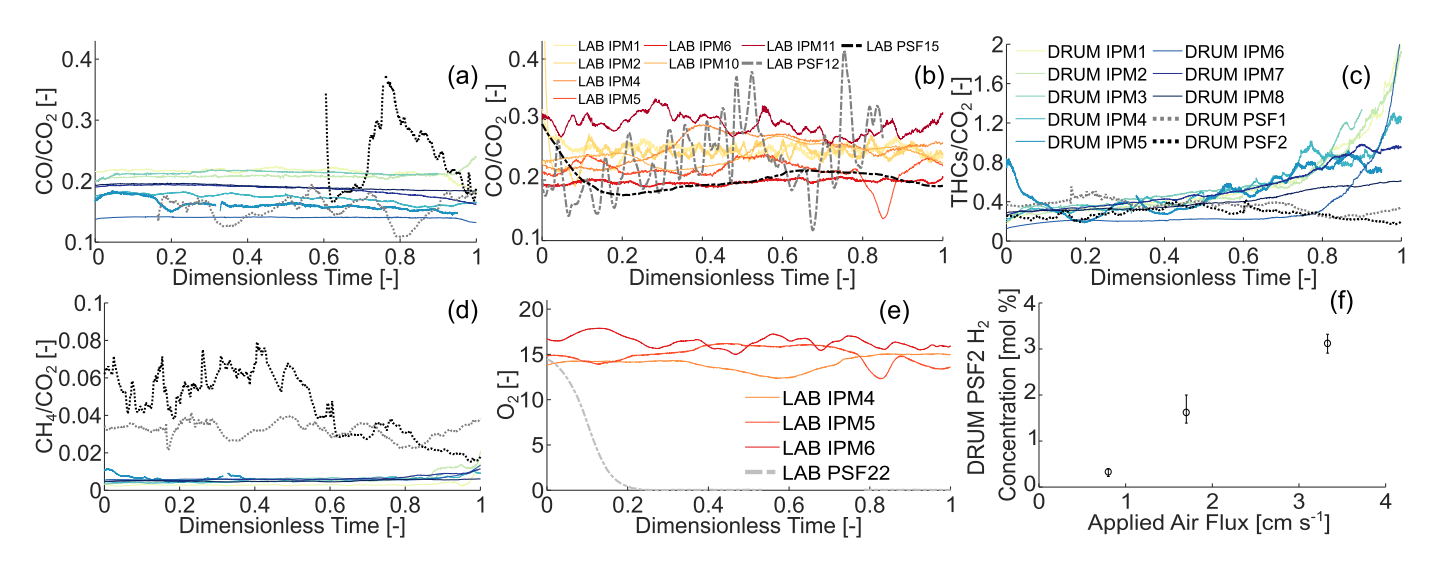


Fig. 6. CO/CO₂ profiles in (a) DRUM and (b) LAB experiments, (c) total hydrocarbons (THCs)/CO₂, and (d) CH₄/CO₂ profiles in DRUM experiments, where the legend in (c) is common to (a), (c), and (d). (e) O₂ measured from select LAB experiments and (f) the H₂ measured from DRUM PSF2 at various points in the experiment with different applied air fluxes, where the error bars note the maximum and minimum values from triplicate measurements. All emissions were measured as vol%.

experiments were above the calibration range (0–0.3%); the other data gaps in Fig. 6 were due to unrepresentative end-effects or experimental adjustments – see additional details in the Supplementary Materials, Section S.5.

Fig. 6a and b show the CO/CO2 fractions from the PSF systems (bolded, black and grey) are roughly comparable to the IPM systems (coloured), between 0.1 and 0.4. These CO/CO2 fractions align with other observations from applied smouldering systems, often 0.05-0.4 [26]. This CO/CO2 range likely reflects the diffusion-limited nature of smouldering in applied systems, i.e., fuel surface oxidation is limited by the rate of oxygen diffusion from the bulk pore space, which therefore drives incomplete oxidation reactions that result in characteristically high fractions of CO/CO₂ [26,28]. Therefore, the common CO/CO₂ range in the IPM and PSF experiments suggests that oxidation may have proceeded similarly in these systems; however, this hypothesis is difficult to confirm. The large scatter in the PSF CO/CO₂ histories is expected to reflect the wider range of endothermic reactions producing CO/CO₂ than in the IPM experiments, as well as the variable nature of the smouldering in those systems due to the fuel bed movement (also seen in the noisy temperature histories in Figs. 3 and 4). In addition, the DRUM IPM CO/CO₂ fractions (Fig. 6a) were lower than the LAB IPM CO/CO₂ fractions (Fig. 6b). This is hypothesized to partially result from the nonuniform air flux in the DRUM IPM experiments, which drove faster airflow velocities near the unreactive reactor wall and led to weaker smouldering with lower propagation velocities, heating rates, and peak temperatures than the LAB IPM experiments [53]. Weaker smouldering can exhibit lower CO/CO2 fractions [49].

Fig. 6c shows the THCs/CO₂ fractions were also similar throughout most of the DRUM PSF and IPM experiments. This result suggests that the pyrolysis regions, where most of the THCs were produced [19,26], were also relatively similar between the IPM and PSF systems. However, the IPM experiments showed large increases in THCs/CO2 near the end of propagation that did not occur in the PSF experiments. These large releases of THCs were due to condensable THCs (volatilized directly from the fuel or produced from pyrolysis or partial oxidation), which recondensed in the cooler porous media ahead of smouldering in the inert heating zone (see a correlation between emissions temperatures and THCs/CO2 in the Supplementary Materials, Section S.8). These condensable THCs accumulated in the IPM experiments and released in high concentrations as the smouldering front reached the end of the fuel bed, which was reported in other smouldering studies using IPM, e.g., [2,22,49,63,64]. This recondensation is absent from DRUM PSF1 and PSF2 systems as their hot emissions (Fig. 2a-c) carried these condensable compounds out of the reactors in the gas phase and prevented the recondensation effect observed in the DRUM IPM experiments.

Fig. 6d shows very different CH_4/CO_2 values throughout the DRUM PSF and IPM experiments, where $10{\text -}100\times$ higher CH_4/CO_2 values were observed in the PSF experiments. This large CH_4 production may be partly due to the fuel differences between the PSF (woodchips and sewage sludge) and IPM (only sewage sludge) experiments, where the woodchips could have released higher fractions of CH_4 upon smouldering than sewage sludge. However, these large differences are also hypothesized to indicate more gasification reactions in the PSF experiments (e.g., the methanation reaction) that drove higher CH_4 production [42].

Fig. 6e shows the key differences in O₂ consumption between IPM and PSF systems. That is, IPM systems with small fuel fractions do not typically consume all available oxygen, unlike PSF systems with large fuel fractions. Oxygen depletion is commonly observed in PSF smouldering systems (e.g., [8,21,65]), which is expected to facilitate an active gasification region that is absent in IPM systems (Fig. 1).

While H_2 is highly uncommon in IPM smouldering experiments, Fig. 6f shows that DRUM PSF2 drove robust H_2 production that increased with applied air flux. This result is hypothesized to occur because the higher air fluxes drove more intense gasification that was responsible for H_2 production. Conversely, in the IPM experiments, H_2

was screened as <1% in the emissions from all DRUM IPM experiments using air fluxes between 1.0 and 15 cm s $^{-1}$; these $\rm H_2$ values are expected to also reflect the LAB IPM experiments (though $\rm H_2$ was not screened). $\rm H_2$ is not routinely measured in IPM smouldering experiments – because it is seldom detected – but $\rm H_2$ is often reported in PSF applied smouldering systems at concentrations between 1 and 10% [19,21,65]. The $\rm H_2$ production in DRUM PSF2 aligns with other PSF smouldering studies and is expected to result from the gasification region in PSF systems (Fig. 1a), which facilitated reactions like the water-gas shift and steammethane-reforming reactions [19,42]. Though these reactions may have also been active to some extent within the IPM systems, the oxygen surplus probably oxidized the intermediate $\rm H_2$ formed, which would explain their low $\rm H_2$ production.

Altogether, Fig. 6 illustrates an important benefit from PSF systems in fostering higher production of useful by-products (e.g., CH_4 and H_2) than IPM systems. Though CH_4 and H_2 differences are influenced by fuel differences to some extent, they both indicate the emergence of an active gasification region characteristic to PSF systems and absent in IPM systems (see Fig. 1). Furthermore, because the CO/CO_2 and $THCs/CO_2$ were similar between the IPM and PSF systems, the other chemical regions (e.g., oxidation and pyrolysis) appear to have proceeded similarly.

4. Conclusions

This experimental study explored the benefits and trade-offs of applied smouldering systems using co-waste mixtures blended with different porous biomass wastes against those with inert porous media (IPM) in various reactors (0.05 to 0.3 m radii). Compared to IPM systems, co-waste systems demonstrated higher throughputs (2–10×), improved scalability (due to thinner cooling zones), straightforward continuous operation (due to smaller inert fractions), and higher production of potentially useful by-products (e.g., $10-100\times$ more CH₄ and up to 3% H₂, which was undetected in IPM systems). However, co-waste systems exhibited lower moisture content limits than IPM systems (\sim 64–71% vs. >74%, respectively).

CRediT authorship contribution statement

Tarek L. Rashwan: Conceptualization, Data curation, Software, Formal analysis, Funding acquisition, Investigation, Methodology, Project administration, Validation, Visualization, Writing - original draft. Taryn Fournie: Data curation, Investigation, Methodology, Project administration, Visualization, Writing - review & editing. Megan Green: Data curation, Investigation, Methodology, Writing review & editing. Alexandra L. Duchesne: Data curation, Investigation, Methodology, Writing - review & editing. Joshua K. Brown: Conceptualization, Data curation, Investigation, Methodology, Writing - review & editing. Gavin P. Grant: Conceptualization, Funding acquisition, Investigation, Methodology, Project administration, Supervision, Writing – review & editing. José L. Torero: Conceptualization, Formal analysis, Investigation, Methodology, Supervision, Project administration, Resources, Writing - review & editing. Jason I. Gerhard: Conceptualization, Funding acquisition, Methodology, Project administration, Resources, Supervision, Writing - review & editing.

Declaration of Competing Interest

The authors declare the following financial interests/personal relationships which may be considered as potential competing interests:

The authors declare the following financial interests/personal relationships which may be considered as potential competing interests: Geosyntec Consultants, through its subsidiary Savron, holds an exclusive license to commercialize smouldering remediation technology. Gavin P. Grant, Alexandra L. Duchesne, and Joshua K. Brown are employed by Geosyntec Consultants, Inc. and Gavin P. Grant is a shareholder in Geosyntec Consultants, Inc.

Data availability

Data will be made available on request.

Acknowledgements

Funding was provided by the Ontario Ministry of Research, Innovation, and Science; the Government of Canada through the Federal Economic Development Agency for Ontario through the Ontario Water Consortium's Advancing Water Technologies Program (Grant SUB02392) with in-kind support from: (i) the Ontario Ministry of the Environment, Conservation and Parks and (ii) Savron (a wholly owned subdivision of Geosyntec Consultants Ltd); the Water Environment Association of Ontario's Residuals and Biosolids Research Fund Award (2018 and 2019); the Natural Sciences and Engineering Research Council of Canada (Canadian Graduate Scholarship – Master's (CGS M) 2017; Postgraduate Scholarship-Doctoral [PGSD3 - 535379-2019 and PGSD3 - 489978-20161 and Grant Nos. CREATE 449311-14. RGPIN 2018-06464, and RGPAS-2018-522602); the Government of Ontario (Ontario Graduate Scholarship 2018); a travel stipend to the first author from the Remediation Education Network Program; and a 2022-23 Higher Education Innovation Funding Knowledge Transfer Voucher from The Open University. We gratefully acknowledge the suggestions from two anonymous reviewers; Jorge Gabayet and Jiahao Wang for performing experiments LAB PSF9-11 and LAB2 PSF22, respectively; and additional project support from Gudgeon Thermfire International (especially from Justin Barfett and Randy Adamski), London Ontario's Greenway Wastewater Treatment Centre (especially from Randy Bartholomew, Michael Wemyss, and Anthony Van Rossum), Cody Murray, Dr. Marco Zanoni, Zia Miry, Anna Toner, Brendan Evers, Thomas Mathias, Dillon McIntyre, Jordan Teeple, Jad Choujaa, Maxwell Servos, Reid Clementino, Kia Barrow, Nick Rogowski, and Christopher Kwan.

Appendix A. Supplementary data

Supplementary data to this article can be found online at https://doi.org/10.1016/j.fuproc.2022.107542.

References

- [1] J.E. Vidonish, K. Zygourakis, C.A. Masiello, G. Sabadell, P.J.J. Alvarez, Thermal treatment of hydrocarbon-impacted soils: a review of technology innovation for sustainable remediation, Engineering 2 (2016) 426–437.
- [2] C. Zhao, Y. Li, Z. Gan, M. Nie, Method of smoldering combustion for refinery oil sludge treatment, J. Hazard. Mater. 409 (2021) 124995.
- [3] Z. Gan, C. Zhao, Y. Li, G. Chen, Z. Song, Z. Zhang, W. Ran, Experimental investigation on smoldering combustion for oil sludge treatment: influence of key parameters and product analysis, Fuel 316 (2022) 123354.
- [4] F.L.F. Bittencourt, M.F. Martins, M.T.D. Orlando, E.S. Galvão, The proof-of-concept of a novel feces destroyer latrine, J. Environ. Chem. Eng. 10 (2022) 106827.
- [5] T.O. Somorin, Valorisation of human excreta for recovery of energy and high-value products: a mini-review, in: M.O. Daramola, A.O. Ayeni (Eds.), Valorization of Biomass to Value-Added Commodities: Current Trends, Challenges, and Future Prospects, Springer International Publishing, Cham, 2020, pp. 341–370.
- [6] J.V.F. Duque, F.L.F. Bittencourt, M.F. Martins, G. Debenest, Developing a combustion-driven reactor for waste conversion, Energy (2021) 121489.
- [7] H.K. Wyn, S. Zárate, J. Carrascal, L. Yermán, A Novel Approach to the Production of Biochar with Improved Fuel Characteristics from Biomass Waste, Waste Biomass Valorization, 2019.
- [8] F.L.F. Bittencourt, G. Debenest, M.F. Martins, Free convection development caused by bed shrinkage in a vacuum-induced smoldering reactor, Chem. Eng. J. (2021) 132847
- [9] R. Pan, G. Debenest, Numerical investigation of a novel smoldering-driven reactor for plastic waste pyrolysis, Energy Convers. Manag. 257 (2022) 115439.
- [10] R. Pan, G. Debenest, M.A.B. Zanoni, Numerical study of plastic waste pyrolysis driven by char smoldering, Process. Saf. Environ. Prot. 165 (2022) 46–56.
- [11] S. Cheng, X. Gao, L. Cao, Q. Wang, Y. Qiao, Quantification of total organic carbon in ashes from smoldering combustion of sewage sludge via a thermal treatment—TGA method, ACS Omega 5 (2020) 33445–33454.
- [12] C. Feng, J. Huang, C. Yang, C. Li, X. Luo, X. Gao, Y. Qiao, Smouldering combustion of sewage sludge: volumetric scale-up, product characterization, and economic analysis, Fuel 305 (2021) 121485.

- [13] C. Feng, M. Cheng, X. Gao, Y. Qiao, M. Xu, Occurrence forms and leachability of inorganic species in ash residues from self-sustaining smouldering combustion of sewage sludge, Proc. Combust. Inst. 38 (2021) 4327–4334.
- [14] Y. Chen, S. Lin, Z. Liang, N.C. Surawski, X. Huang, Smouldering organic waste removal technology with smoke emissions cleaned by self-sustained flame, J. Clean. Prod. 362 (2022) 132363.
- [15] Z. Song, T. He, M. Li, D. Wu, F. You, Self-sustaining smoldering as a novel disposal approach for food waste with high moisture content, Fuel Process. Technol. 228 (2022) 107144.
- [16] Y. Chen, S. Lin, Z. Liang, X. Huang, Clean smoldering biowaste process: effect of burning direction on smoke purification by self-sustained flame, Fuel Process. Technol. 237 (2022) 107453.
- [17] T. Fournie, T.L. Rashwan, C. Switzer, J.I. Gerhard, Phosphorus recovery and reuse potential from smouldered sewage sludge ash, Waste Manag. 137 (2022) 241–252.
- [18] A.H. Ezieke, A. Serrano, W. Clarke, D.K. Villa-Gomez, Bottom ash from smouldered digestate and coconut coir as an alkalinity supplement for the anaerobic digestion of fruit waste, Chemosphere 296 (2022) 134049.
- [19] H.K. Wyn, M. Konarova, J. Beltramini, G. Perkins, L. Yermán, Self-sustaining smouldering combustion of waste: a review on applications, key parameters and potential resource recovery, Fuel Process. Technol. 205 (2020) 106425.
- [20] S. Yan, D. Yin, F. He, J. Cai, T. Schliermann, F. Behrendt, Characteristics of smoldering on moist rice husk for silica production, Sustainability 14 (2022) 317.
- [21] A. Serrano, H. Wyn, L. Dupont, D.K. Villa-Gomez, L. Yermán, Self-sustaining treatment as a novel alternative for the stabilization of anaerobic digestate, J. Environ. Manag. 264 (2020) 110544.
- [22] L. Yermán, R.M. Hadden, J. Carrascal, I. Fabris, D. Cormier, J.L. Torero, J. I. Gerhard, M. Krajcovic, P. Pironi, Y.-L. Cheng, Smouldering combustion as a treatment technology for faeces: exploring the parameter space, Fuel 147 (2015) 108–116.
- [23] P. Pironi, C. Switzer, G. Rein, A. Fuentes, J.I. Gerhard, J.L. Torero, Small-scale forward smouldering experiments for remediation of coal tar in inert media, Proc. Combust. Inst. 32 (2009) 1957–1964.
- [24] C. Switzer, P. Pironi, J.I. Gerhard, G. Rein, J.L. Torero, Volumetric scale-up of smouldering remediation of contaminated materials, J. Hazard. Mater. 268 (2014) 51–60.
- [25] M. Salman, J.I. Gerhard, D.W. Major, P. Pironi, R. Hadden, Remediation of trichloroethylene-contaminated soils by star technology using vegetable oil smoldering, J. Hazard. Mater. 285 (2015) 346–355.
- [26] J.L. Torero, J.I. Gerhard, M.F. Martins, M.A.B. Zanoni, T.L. Rashwan, J.K. Brown, Processes defining smouldering combustion: Integrated review and synthesis, Prog. Energy Combust. Sci. 81 (2020) 100869.
- [27] T.J. Ohlemiller, Modeling of smoldering combustion propagation, Prog. Energy Combust. Sci. 11 (1985) 277–310.
- [28] G. Gianfelice, P. Canu, On the mechanism of single pellet smouldering combustion, Fuel 301 (2021) 121044.
- [29] Z. Song, Modelling oxygen-limited and self-sustained smoldering propagation: Underground coal fires driven by thermal buoyancy, Combust. Flame 245 (2022) 112382.
- [30] X. Huang, G. Rein, Thermochemical conversion of biomass in smouldering combustion across scales: the roles of heterogeneous kinetics, oxygen and transport phenomena, Bioresour. Technol. 207 (2016) 409–421.
- [31] M.A.B. Zanoni, G. Rein, L. Yermán, J.I. Gerhard, Thermal and oxidative decomposition of bitumen at the microscale: kinetic inverse modelling, Fuel 264 (2020) 116704.
- [32] J.I. Gerhard, G.P. Grant, J.L. Torero, Chapter 9 Star: a uniquely sustainable in situ and ex situ remediation process, in: D. Hou (Ed.), Sustainable Remediation of Contaminated Soil and Groundwater, Butterworth-Heinemann, 2020, pp. 221–246.
- [33] A.L. Duchesne, J.K. Brown, D.J. Patch, D. Major, K.P. Weber, J.I. Gerhard, Remediation of PFAS-contaminated soil and granular activated carbon by smoldering combustion, Environ. Sci. Technol. 54 (2020) 12631–12640.
- [34] T.L. Rashwan, J.I. Gerhard, G.P. Grant, Application of self-sustaining smouldering combustion for the destruction of wastewater biosolids, Waste Manag. 50 (2016) 201–212
- [35] G. Gianfelice, M. Della Zassa, A. Biasin, P. Canu, Onset and propagation of smouldering in pine bark controlled by addition of inert solids, Renew. Energy 132 (2019) 596–614.
- [36] R. Solinger, G.P. Grant, G.C. Scholes, C. Murray, J.I. Gerhard, STARx Hottpad for smoldering treatment of waste oil sludge: proof of concept and sensitivity to key design parameters, Waste Manag. Res. 38 (2020) 554–566.
- [37] R.B. Morales, C.T. DeGroot, G.C. Scholes, J.I. Gerhard, Understanding, controlling and optimising the cooling of waste thermal treatment beds including STARx Hottpads, Waste Manag. Res. 40 (9) (2022) 1390–1401, 0734242X221076308.
- [38] E.A. Salgansky, A.Y. Zaichenko, D.N. Podlesniy, M.V. Salganskaya, M. Toledo, Coal dust gasification in the filtration combustion mode with syngas production, Int. J. Hydrog. Energy 42 (2017) 11017–11022.
- [39] E.A. Salgansky, A.Y. Zaichenko, D.N. Podlesniy, M.V. Salganskaya, M.V. Tsvetkov, A.V. Chub, Gasification of oil shale dust in a counterflow moving bed filtration combustion reactor, Int. J. Hydrog. Energy 45 (2020) 17270–17275.
- [40] M. Abdul Mujeebu, Hydrogen and syngas production by superadiabatic combustion – a review, Appl. Energy 173 (2016) 210–224.
- [41] N. Gao, K. Kamran, C. Quan, P.T. Williams, Thermochemical conversion of sewage sludge: a critical review, Prog. Energy Combust. Sci. 79 (2020) 100843.
- [42] P. Basu, Biomass Gasification and Pyrolysis: Practical Design and Theory, Academic Press, Oxford, 2010.
- [43] L. Zhang, C. Xu, P. Champagne, Overview of recent advances in thermo-chemical conversion of biomass, Energy Convers. Manag. 51 (2010) 969–982.

- [44] S.Z. Miry, M.A.B. Zanoni, T.L. Rashwan, J.L. Torero, J.I. Gerhard, Investigation of multi-dimensional transfer effects in applied smouldering systems: a 2D numerical modelling approach, Combust. Flame 246 (2022) 112385.
- [45] M.A.B. Zanoni, J. Wang, J.L. Torero, J.I. Gerhard, Multiphase modelling of water evaporation and condensation in an air-heated porous medium, Appl. Therm. Eng. (2022) 118516.
- [46] M.A.B. Zanoni, J.L. Torero, J.I. Gerhard, The role of local thermal non-equilibrium in modelling smouldering combustion of organic liquids, Proc. Combust. Inst. 37 (2019) 3109–3117.
- [47] T.L. Rashwan, J.L. Torero, J.I. Gerhard, Heat losses in applied smouldering systems: sensitivity analysis via analytical modelling, Int. J. Heat Mass Transf. 172 (2021) 121150
- [48] T.L. Rashwan, J.L. Torero, J.I. Gerhard, Heat losses in a smouldering system: the key role of non-uniform air flux, Combust. Flame 227 (2021) 309–321.
- [49] T.L. Rashwan, J.L. Torero, J.I. Gerhard, The improved energy efficiency of applied smouldering systems with increasing scale, Int. J. Heat Mass Transf. 177 (2021) 121548
- [50] Z. Lu, Structure and extinction of reverse smolder waves in the presence of heat losses: a premixed-flame perspective, Combust. Flame 242 (2022) 112201.
- [51] J.L. Ellzey, E.L. Belmont, C.H. Smith, Heat recirculating reactors: fundamental research and applications, Prog. Energy Combust. Sci. 72 (2019) 32–58.
- [52] M.A.B. Zanoni, J.L. Torero, J.I. Gerhard, Determining the conditions that lead to self-sustained smouldering combustion by means of numerical modelling, Proc. Combust. Inst. 37 (2019) 4043–4051.
- [53] T.L. Rashwan, T. Fournie, J.L. Torero, G.P. Grant, J.I. Gerhard, Scaling up self-sustained smouldering of sewage sludge for waste-to-energy, Waste Manag. 135 (2021) 298–308.
- [54] S. Lin, Y.K. Cheung, Y. Xiao, X. Huang, Can rain suppress smoldering peat fire? Sci. Total Environ. 727 (2020) 138468.

- [55] R.M. Hadden, G. Rein, C.M. Belcher, Study of the competing chemical reactions in the initiation and spread of smouldering combustion in peat, Proc. Combust. Inst. 34 (2013) 2547–2553.
- [56] M.A.B. Zanoni, J. Wang, J.I. Gerhard, Understanding pressure changes in smouldering thermal porous media reactors, Chem. Eng. J. 412 (2021) 128642.
- [57] L. Kinsman, J.L. Torero, J.I. Gerhard, Organic liquid mobility induced by smoldering remediation, J. Hazard. Mater. 325 (2017) 101–112.
- [58] J. Wang, G.P. Grant, J.I. Gerhard, The influence of porous media heterogeneity on smouldering remediation, J. Contam. Hydrol. 237 (2021) 103756.
- [59] M.A.B. Zanoni, J.L. Torero, J.I. Gerhard, Determination of the interfacial heat transfer coefficient between forced air and sand at Reynold's numbers relevant to smouldering combustion, Int. J. Heat Mass Transf. 114 (2017) 90–104.
- [60] M.A.B. Zanoni, J.L. Torero, J.I. Gerhard, Delineating and explaining the limits of self-sustained smouldering combustion, Combust. Flame 201 (2019) 78–92.
- [61] I. Fabris, D. Cormier, J.I. Gerhard, T. Bartczak, M. Kortschot, J.L. Torero, Y.-L. Cheng, Continuous, self-sustaining smouldering destruction of simulated faeces, Fuel 190 (2017) 58–66.
- [62] D. Podlesniy, A. Zaichenko, M. Tsvetkov, M. Salganskaya, A. Chub, E. Salgansky, Experimental investigation of waste oil processing by partial oxidation in a moving bed reactor, Fuel 298 (2021) 120862.
- [63] M.F. Martins, S. Salvador, J.F. Thovert, G. Debenest, Co-current combustion of oil shale – part 2: structure of the combustion front, Fuel 89 (2010) 133–143.
- [64] T. Fournie, T.L. Rashwan, C. Switzer, G.P. Grant, J.I. Gerhard, Exploring PCDD/Fs and potentially toxic elements in sewage sludge during smouldering treatment, J. Environ. Manag. 317 (2022) 115384.
- [65] F.A.F. Monhol, M.F. Martins, Cocurrent combustion of human feces and polyethylene waste, Waste Biomass Valorization 6 (2015) 425–432.